Progress In Electromagnetics Research B, Vol. 118, 30–41, 2026

PIER B

(Received 14 May 2026, Accepted 29 June 2026, Scheduled 20 July 2026)

Well-Posed and Effective High-Order Absorbing Boundary Conditions for the Time-Harmonic Solution of Maxwell's Equations

Bruno Stupfel*

CEA, DAM, CESTA, F-33114 Le Barp, France

ABSTRACT: For the time-harmonic solution of Maxwell's equations, absorbing boundary conditions (ABCs) are widely used to approximate the Silver-Müller radiation condition at infinity on the boundary Γ terminating the computational domain. An original high-order ABC (HOABC) is proposed that links the tangential components of the electric and magnetic fields on Γ via surface differential operators multiplied by coefficients. These coefficients are determined so as to minimize the reflection of a propagative or evanescent wave incident on a planar or spherical Γ — while taking its radius into account — and guarantee a well-posed Maxwell's problem. Numerical results are presented on a plane and coated spheres that demonstrate its efficiency even when evanescent waves are present. If it is implemented in a finite element formulation, its numerical complexity is expected to be low.

1. INTRODUCTION

The finite element method (FEM) is widely employed for the solution of 3-D time-harmonic electromagnetic problems involving heterogeneous objects [1–3]. One of the main difficulties involved is taking into account the Silver-Müller radiation condition at infinity on the outer boundary Γ terminating the computational domain Ω enclosing the objects. This can be done by implementing either (i) an exact condition, typically an integral equation (integral equation (IE): see, e.g., [4–7]) or an approximate one, such as (ii) a perfectly matched layer (PML), see, e.g., [8–11], or else (iii) an absorbing boundary condition (ABC), see, e.g., [2, 12–18]. The first approach is computationally intensive, and the second can lead to an ill-conditioned finite element (FE) matrix, which slows the convergence of iterative methods used to solve large FE systems [19–21]. Regarding the ABC, it is all the more efficient since the distance d between Γ and the object is large, thereby involving a large computational domain and increasing the numerical burden of the FE solution.

An ABC links the tangential components on Γ of the electric and magnetic fields. An exact radiation condition, like the above-mentioned IE, is nonlocal. To introduce non-locality and hence increase its effectiveness and decrease d, high-order ABCs (HOABCs) have been proposed for the time-harmonic Maxwell's problem [16–18]. Their efficiency is often measured in the spectral domain by the reflection coefficient of a planar wave incident on a planar Γ. Other important issues in the HOABC's choice are its well-posedness (uniqueness of solutions to Maxwell's problem must be guaranteed), its ease of numerical implementation, and the induced computational cost. For the field scattered from an object illuminated by an incident wave or the total field radiated from a source inside Ω, an ABC is an impedance boundary condition (IBC) prescribed on Γ located in free space.

We consider in this paper an original HOABC obtained from the high-order impedance boundary condition (HOIBC) presented in [22]: the tangential components of the electric and magnetic fields on Γ are connected via surface differential operators multiplied by coefficients. If it is implemented in an FE formulation, its numerical complexity is expected to be low, similar to that of the above-mentioned HOIBC. The HOABC coefficients are determined so as to minimize the reflection of a propagative or evanescent wave incident on a planar or spherical Γ and guarantee a well-posed Maxwell's problem. The organization of this paper is as follows. Section 2 first presents the generic HOABC formulation. Then, the HOABC's coefficients are computed in Section 2.1 when Γ is an infinite plane and in Section 2.2 when Γ is a sphere. In Section 2.1, Γ is illuminated by incident propagative (planar homogeneous) or evanescent (planar inhomogeneous) waves. The coefficients are obtained by minimizing the reflected wave amplitude in both TM and TE polarizations. They can be used on an arbitrary Γ by invoking the tangent plane approximation (PA): at any point on Γ, the surface is replaced by the plane tangent to Γ at this point. In Section 2.2, Γ is a sphere illuminated by an arbitrary inner source. The problem is solved via the well-known Mie series, and the HOABC coefficients are obtained by minimizing the wave spuriously reflected by Γ, while taking into account its radius. This calculation process is termed in what follows spherical approximation (SA). Sufficient uniqueness conditions (SUCs) are derived in Section 2.3 from those proposed in [22] for the HOIBC. To guarantee a well-posed HOAB, they can be used as constraints in the minimization processes that yield the coefficient

* Corresponding author: Bruno Stupfel (bruno.stupfel@cea.fr).

doi:10.2528/PIERB26051401

values, as described in Sections 2.1 and 2.2. Various ABCs derived from the generic HOABC are proposed whose performances are numerically evaluated in Section 2.4 when Γ is a plane or a sphere. Time dependence $\exp(i\omega t)$ is assumed and suppressed throughout.

2. HOABC FORMULATION

We recall that the HOIBC in [22] reads

$$L_E \underline{E}_t + L_J \underline{J} = 0 \text{ on } \Gamma \tag{1}$$

with

$$L_E = 1 + \frac{b_1}{k^2} L_D - \frac{b_2}{k^2} L_R;\ L_J = a_0 + \frac{a_1}{k^2} L_D - \frac{a_2}{k^2} L_R \tag{2}$$

$k = 2\pi/\lambda = \omega/c$ is the free-space wave number (c is the light velocity); $(\underline{E}, \underline{H})$ is the total field (in this paper, $\underline{H}$ stands for $\eta_0 \underline{H}$ with η_0 being the free-space impedance); subindex t indicates the tangential components of a vector or operator, and $\underline{J} = \underline{n} \times \underline{H}$ with $\underline{n}$ being he outward directed normal to Γ. The tangential operators L_D, L_R are defined as

$$\begin{aligned} &\underline{V}_t = -\underline{n} \times (\underline{n} \times \underline{V});\ L_D \underline{V}_t = \underline{\nabla}_t \nabla_t \cdot \underline{V}_t; \\ &L_R \underline{V}_t = \underline{curl}_\Gamma curl_\Gamma \underline{V}_t;\ curl_\Gamma \underline{V}_t = -\underline{\nabla}_t \cdot (\underline{n} \times \underline{V}_t); \\ &\underline{curl}_\Gamma u = -\underline{n} \times \underline{\nabla}_t u \end{aligned} \tag{3}$$

where u is a scalar. For a radiation problem (sources inside Ω), $(\underline{E}, \underline{H})$ is the total radiated field, and (1) is the HOABC on Γ. For a scattering problem, if $(\underline{E}^s, \underline{H}^s)$ designates the field scattered from the object, the HOABC on Γ is

$$L_E \underline{E}_t^s + L_J \underline{J}^s = 0 \text{ on } \Gamma \tag{4}$$

with $\underline{J}^s = \underline{n} \times \underline{H}^s$. Sections 2.1 and 2.2 present the computing process of the HOABC coefficients in the PA and SA. SUCs are proposed in Section 2.3 for the HOABC. The performances of the various ABCs derived from the generic HOABC in (4) are numerically evaluated in Section 2.4 on an infinite planar boundary and on a spherical one.

2.1. Computation of the HOABC Coefficients in (2) in the Planar Approximation (PA)

In this section, we consider the standard model problem where a propagative or evanescent wave with amplitude 1 illuminates a planar Γ: $(\underline{E}, \underline{H})$ is the sum of this incident field and of the spuriously reflected wave with amplitude r. Γ is the (xOy) plane. and $\underline{n}$ is directed along the negative z axis. The fields are y independent with the following Cartesian components in TM and TE polarizations and for $z \geq 0$:

$$\begin{aligned} &\text{TM: } \underline{H} = (0, H, 0)^t,\ \underline{E} = \frac{i}{k}(\partial_z H, 0, -\partial_x H)^t;\ H = H_y \\ &\quad \underline{J} = (-H, 0, 0)^t \\ &\text{TE: } \underline{E} = (0, E, 0)^t,\ \underline{H} = -\frac{i}{k}(\partial_z E, 0, -\partial_x E)^t;\ E = E_y \\ &\quad \underline{J} = (0, H_x, 0)^t \end{aligned} \tag{5}$$

We have

$$\begin{aligned} &\text{TE: } E = e^{iksx}(e^{izk\xi} + r^{\text{TE}} e^{-izk\xi}); \\ &\text{TM: } H = e^{iksx}(e^{izk\xi} - r^{\text{TM}} e^{-izk\xi}) \\ &\text{TE: } H_x = \xi e^{iksx}(e^{izk\xi} - r^{\text{TE}} e^{-izk\xi}); \\ &\text{TM: } E_x = -\xi e^{iksx}(e^{izk\xi} + r^{\text{TM}} e^{-izk\xi}) \\ &s \leq 1:\ \xi = \sqrt{1 - s^2};\ s > 1: \xi = -i\sqrt{s^2 - 1} \end{aligned} \tag{6}$$

The first r.h.s. term in the above expressions of E and H is the incident wave and the second one the spuriously reflected wave. Parameter s in (6) characterizes these waves: if $s \leq 1$, they are propagative (planar homogeneous) with $s = \sin\theta$, where θ is the real incidence angle counted from the z axis; if $s > 1$, they are evanescent (planar inhomogeneous) and $\text{Im}(\xi) \leq 0$ in order to satisfy the radiation condition. The latter are considered because evanescent waves might be impinging on Γ if it is located close to the object. Substituting (5) and (6) into (1) successively for both polarizations, we get

$$\underline{E}_t = \begin{pmatrix} Z^{\text{TM}} & 0 \\ 0 & Z^{\text{TE}} \end{pmatrix} \underline{J} \tag{7}$$

with

$$\begin{aligned} Z^{\text{TM}} &= \frac{a_0 - a_1 s^2}{1 - b_1 s^2};\quad Z^{\text{TE}} = \frac{a_0 - a_2 s^2}{1 - b_2 s^2} \\ r^{\text{TM}} &= \frac{Z^{\text{TM}} - \xi}{Z^{\text{TM}} + \xi};\quad r^{\text{TE}} = \frac{\xi Z^{\text{TE}} - 1}{\xi Z^{\text{TE}} + 1} \end{aligned} \tag{8}$$

Note that r^{TM}, r^{TE} depend on s and $\chi = (a_0, a_1, a_2, b_1, b_2)^t \in \mathbb{C}^5$. The spurious reflection on Γ in both polarizations is minimized for $s \in [0, s_M]$ when $\chi^{\text{PA}} = \arg\min\{\sum_{p=\text{TM,TE}} \int_0^{s_M} |r^p(s, \chi)| ds\}$ (note that when $s_M > 1$, evanescent waves are taken into account). χ^{PA} is approximated by

$$\chi^{\text{PA}} = \arg\min\left\{\sum_{p=\text{TM,TE}} \sum_{i=1}^{N_{s_M}} |r^p(s_i, \chi)|\right\};\ s_{N_{s_M}} = s_M \tag{9}$$

where s_i are uniformly distributed in $[0, s_M]$. We show in Appendix A that

$$Z^{\text{TM}}(s, \chi) = 1/Z^{\text{TE}}(s, \chi) \tag{10}$$

minimizes $\sum_{p=\text{TM,TE}} |r^p(s, \chi)|$. This entails $r^{\text{TM}}(s, \chi) = -r^{\text{TE}}(s, \chi)$ and is satisfied for all s if we set $a_0 = 1$, $b_2 = a_1$, $b_1 = a_2$. We have numerically verified via (9) that $|a_0 - 1|$, $|b_2 - a_1|$ and $|b_1 - a_2|$ are actually very small for any value of s_M. For this reason, we set a particular HOABC, termed ABC3, as

$$\begin{aligned} \text{ABC3}:\ & a_0 = 1,\ b_2 = a_1,\ b_1 = a_2 \Longrightarrow r^{\text{TM}}(s, \chi) \\ & = -r^{\text{TE}}(s, \chi)\,\forall s \end{aligned} \tag{11}$$

Also, it is of interest to evaluate the performance of the following ABCs:

$$\text{ABC0}: a_0 = 1,\ a_1 = a_2 = b_1 = b_2 = 0 \Longrightarrow r^{\text{TM}}(s)$$

$$
\begin{aligned}
&= -r^{\mathrm{TE}}(s)\\
&\mathrm{ABC1}: a_0 = 1,\ b_1 = b_2 = 0\\
&\mathrm{ABCWK}: a_0 = 1,\ a_1 = \frac{1}{2(1-i/kR)},\ a_2 = -a_1,\\
&\qquad b_1 = b_2 = 0\\
&\mathrm{ABC2}: a_0 = 1,\ a_1 = a_2 = 0\\
&\mathrm{ABC30}: a_0 = 1,\ a_1 = b_2 = 3/4,\ a_2 = b_1 = 1/4\\
&\qquad \Longrightarrow r^{\mathrm{TM}}(s,\chi) = -r^{\mathrm{TE}}(s,\chi) \qquad (12)
\end{aligned}
$$

ABC0 is the standard zero-order ABC that satisfies (10) and is exact for a propagative plane wave in normal incidence on Γ ($s = 0$). Absorbing boundary condition (ABCWK) is proposed in [17] where R is the radius of Γ when it is a sphere; when it is planar, $kR = \infty$ so that $a_1 = 1/2 = -a_2$. If (10) is satisfied, we show in Appendix B that ABC30 results from the Padé approximant centered at $s = 0$ of the exact ABC pseudo-differential operator symbol derived in this Appendix for a planar Γ. It can be considered as the 3D vector equivalent of the third approximation of the exact 2D scalar ABC proposed in [13] (see also [14]). For the generic HOABC, we set $Z^{\mathrm{TM}}(s_i,\chi) = 1/Z^{\mathrm{TE}}(s_i,\chi) = \xi_i$ that, because of (8), entails $r^{\mathrm{TM}}(s_i,\chi) = r^{\mathrm{TE}}(s_i,\chi) = 0$, and χ is the solution of the following least square $(2N_{s_M} \times 5)$ system

$$
\begin{aligned}
&a_0 - a_1 s_i^2 + b_1 s_i^2 \xi_i = \xi_i \quad a_0 - a_2 s_i^2 + b_2 s_i^2/\xi_i = 1/\xi_i\\
&s_i \le 1 : \xi_i = \sqrt{1-s_i^2};\ s_i > 1 : \xi_i = -i\sqrt{s_i^2-1} \qquad (13)
\end{aligned}
$$

On account of the definitions (12) and (11), (13) is reduced to a $(2N_{s_M} \times 2)$ system for ABC1, ABC2

$$
\begin{aligned}
\mathrm{ABC1}: &\ 1 - a_1 s_i^2 = \xi_i\\
&\ 1 - a_2 s_i^2 = 1/\xi_i\\
\mathrm{ABC2}: &\ 1 + b_1 s_i^2 \xi_i = \xi_i\\
&\ 1 + b_2 s_i^2/\xi_i = 1/\xi_i
\end{aligned} \qquad (14)
$$

and an $(N_{s_M} \times 2)$ system for ABC3 (the first line is only kept in (13) since $b_1 = a_2$)

$$1 - a_1 s_i^2 + a_2 s_i^2 \xi_i = \xi_i \qquad (15)$$

Regarding ABC1 and ABC2, we note that the two systems in (14) yield $b_1 = a_2$, $b_2 = a_1$ if s_i are the same so that, on account of (8),

$$
\begin{aligned}
&Z^{\mathrm{TM}}_{\mathrm{ABC1}}(s_i,\chi) = 1/Z^{\mathrm{TE}}_{\mathrm{ABC2}}(s_i,\chi);\\
&Z^{\mathrm{TE}}_{\mathrm{ABC1}}(s_i,\chi) = 1/Z^{\mathrm{TM}}_{\mathrm{ABC2}}(s_i,\chi)\\
&\Longrightarrow\\
&r^{\mathrm{TM}}_{\mathrm{ABC1}}(s_i,\chi) = -r^{\mathrm{TE}}_{\mathrm{ABC2}}(s_i,\chi);\\
&r^{\mathrm{TE}}_{\mathrm{ABC1}}(s_i,\chi) = -r^{\mathrm{TM}}_{\mathrm{ABC2}}(s_i,\chi)
\end{aligned} \qquad (16)
$$

which means that ABC1 and ABC2 have exactly the same efficiency. For the same reason, ABCWK in (12) has the same efficiency if $a_0 = 1$, $b_2 = 1/[2(1-i/kR)]$, $b_1 = -b_2$, $a_1 = a_2 = 0$. Also, for ABC1, when $s \to 0$, (14) yields $1 - a_1 s^2 \simeq 1 - s^2/2$, $1 - a_2 s^2 \simeq 1 + s^2/2$ that implies $a_1 = -a_2 = 1/2$ (this is actually what is numerically obtained from (14) when $s_M \to 0$), thus recovering ABCWK: ABCWK $=$ ABC1($s_M = 0$).

Regarding ABC3, we have numerically verified that, when $s_M \to 0$, (13) actually yields the ABC30 coefficients in (12): ABC30 $=$ ABC3($s_M = 0$).

Finally, because $\xi \in \mathbb{R}$, when $s \le 1$, (8) entails, for $p =$ TM, TE,

$$s \le 1 : \ \mathrm{Re}(Z^p(s)) \ge 0 \Longrightarrow |r^p(s)| \le 1 \qquad (17)$$

Also, for each of the above ABCs and for $p =$ TM, TE, we have

$$|r^p(s=1)| = 1\,;\ \lim_{s\to\infty} |r^p(s)| = 1 \qquad (18)$$

$$\chi \in \mathbb{R}^5 \Longrightarrow |r^p(s>1)| = 1 \qquad (19)$$

Depending on the type of waves present on Γ, (17) shows that all the ABCs defined in (11) and (12) can be efficient for propagative waves, while (18) indicates that ABC1 $=$ ABC2, ABC3 is unusable for weakly or highly evanescent waves, and (19) shows that ABC0, ABCWK, ABC30 fail completely for all evanescent waves.

2.2. Computation of the HOABC Coefficients in (2) in the Spherical Approximation (SA)

In this section, Γ is a sphere of radius R, and an arbitrary source located inside Γ radiates an outgoing wave that, when reflected by Γ, produces a (spurious) incoming wave. The total field $(\underline{E},\underline{H})$ inside Γ is given by the standard Mie series

$$
\begin{aligned}
\underline{E}(\underline{r}) &= \sum_{n=0}^{\infty}\sum_{|m|\le n}[\overline{\alpha}_{mn}\underline{\overline{M}}_{mn}(\underline{r}) + \overline{\beta}_{mn}\underline{\overline{N}}_{mn}(\underline{r})]\\
&\quad + \sum_{n=0}^{\infty}\sum_{|m|\le n}[\alpha_{mn}\underline{M}_{mn}(\underline{r}) + \beta_{mn}\underline{N}_{mn}(\underline{r})]\\
\underline{H}(\underline{r}) &= i\sum_{n=0}^{\infty}\sum_{|m|\le n}[\overline{\beta}_{mn}\underline{\overline{M}}_{mn}(\underline{r}) + \overline{\alpha}_{mn}\underline{\overline{N}}_{mn}(\underline{r})]\\
&\quad + i\sum_{n=0}^{\infty}\sum_{|m|\le n}[\beta_{mn}\underline{M}_{mn}(\underline{r}) + \alpha_{mn}\underline{N}_{mn}(\underline{r})]
\end{aligned} \qquad (20)
$$

with

$$
\begin{aligned}
\underline{\overline{M}}_{mn}(\underline{r}) &= \underline{\nabla} \times (\underline{r}\overline{\Psi});\ \underline{\overline{N}}_{mn}(\underline{r}) = \underline{\nabla} \times \underline{\overline{M}}_{mn}(\underline{r})/k\\
\overline{\Psi} &= h_n(kr)P_n^m(\cos\theta)e^{im\varphi}
\end{aligned} \qquad (21)
$$

$h_n(x)$ is the spherical Hankel function of the second kind and $P_n^m(\cos\theta)$ the Legendre function. The same definitions hold for $\underline{M}_{mn}$ and $\underline{N}_{mn}$, where the spherical Bessel function $j_n(x)$ is substituted to $h_n(x)$. Coefficients $\overline{\alpha}_n, \overline{\beta}_n$ (α_n, β_n) correspond to the outgoing (respectively incoming) wave. Because $(\underline{E},\underline{H})$ satisfies the HOABC that is here the HOIBC (1), we get

$$
\begin{aligned}
\alpha_{mn} &= -\overline{\alpha}_{mn}D_n^a;\ \beta_{mn} = -\overline{\beta}_{mn}D_n^b\\
D_n^a &= \frac{iZ_{2n}\widetilde{h}_n(x) - xh_n(x)}{iZ_{2n}\widetilde{j}_n(x) - xj_n(x)};
\end{aligned}
$$

$$D_n^b = \frac{iZ_{1n}xh_n(x) + \widetilde{h}_n(x)}{iZ_{1n}xj_n(x) + \widetilde{j}_n(x)};\ x = kR$$

$$Z_{1n} = \frac{a_0 - \gamma_n a_1}{1 - \gamma_n b_1};\ Z_{2n} = \frac{a_0 - \gamma_n a_2}{1 - \gamma_n b_2};\ \gamma_n = \frac{n(n+1)}{x^2}$$

$$\widetilde{j}_n(x) = \frac{d}{dx}(xj_n(x));\ \widetilde{h}_n(x) = \frac{d}{dx}(xh_n(x)) \tag{22}$$

As in Section 2.1, the objective is to compute the ABCs coefficients, represented by the set $\chi = (a_0, a_1, a_2, b_1, b_2)^t \in \mathbb{C}^5$, which minimize the reflected wave, i.e., minimize $|\alpha_{mn}(\chi)| + |\beta_{mn}(\chi)|$ for $0 \le n \le n_M$, $|m| \le n$. n_M is considered a parameter that plays a similar role to parameter s_M introduced in Section 2.1 for the planar approximation and is determined as follows. If $R_S \le R$ is the radius of the sphere circumscribed to the object, the field radiated from it or scattered by it reads, for $r \ge R_S$,

$$\begin{aligned} \underline{E}(\underline{r}) &= \sum_{n=0}^{\infty}\sum_{|m|\le n}[c_{mn}\overline{M}_{mn}(\underline{r}) + d_{mn}\overline{N}_{mn}(\underline{r})] \\ \underline{H}(\underline{r}) &= i\sum_{n=0}^{\infty}\sum_{|m|\le n}[d_{mn}\overline{M}_{mn}(\underline{r}) + c_{mn}\overline{N}_{mn}(\underline{r})] \end{aligned} \tag{23}$$

(for simplicity's sake, coefficients c_{mn}, d_{mn} are not elaborated here). Because a plane wave is evanescent in z when $s \ge 1$ and $\overline{M}_{mn}(\underline{r})$, $\overline{N}_{mn}(\underline{r})$ are evanescent in r for $n > kr \gg 1$ [24], we get the following approximate equivalence between PA and SA:

$$kR_S \gg 1:\ s \equiv \frac{n}{kR_S} \tag{24}$$

In view of (22), we have

$$\chi^{\text{SA}} = \arg\min\left\{\sum_{n=1}^{n_M}(|D_n^a(\chi)| + |D_n^b(\chi)|)\right\} \tag{25}$$

If we let

$$n_M = E(s_M kR_S) + 1 \tag{26}$$

(E is for the integer part), then evanescent spherical waves issued from the object will be accounted for on Γ if $s_M \ge 1$. On the other hand, we have the following results:

1) If we set $f(Z_{1n}, Z_{2n}) = |D_n^a(\chi)| + |D_n^b(\chi)|$, then f verifies $f(Z_{1n}, Z_{2n}) = f(1/Z_{2n}, 1/Z_{1n})$ because of (22), and it follows from Appendix A that the minimum of f is achieved for $Z_{1n} = 1/Z_{2n}$: we recover the PA definition (11) of ABC3 where $r^{\text{TM}}(s,\chi) = -r^{\text{TE}}(s,\chi)\ \forall s$ is replaced by

$$D_n^a = D_n^b\ \forall n \tag{27}$$

(27) and (22) with $b_1 = a_2$, $b_2 = a_1$ yield the $(n_M, 2)$ system

$$0 \le n \le n_M\ ;\ x = kR$$
$$\frac{i\dfrac{1-\gamma_n a_2}{1-\gamma_n a_1}\widetilde{h}_n(x) - xh_n(x)}{i\dfrac{1-\gamma_n a_2}{1-\gamma_n a_1}\widetilde{j}_n(x) - xj_n(x)} = \frac{i\dfrac{1-\gamma_n a_1}{1-\gamma_n a_2}xh_n(x) + \widetilde{h}_n(x)}{i\dfrac{1-\gamma_n a_1}{1-\gamma_n a_2}xj_n(x) + \widetilde{j}_n(x)} \tag{28}$$

whose least-squares solution gives the SA values of a_1 and a_2.

2) As a consequence, regarding ABC0, we set $a_0 = 1$ independent of R: ABC0 cannot take the curvature into account. Also, if the source is an electric dipole located at the origin, the outgoing wave satisfies $(\underline{E}, \underline{H}) \propto (\overline{N}_{01}(\underline{r}), \overline{M}_{01}(\underline{r}))$ [27] so that $\overline{\alpha}_{mn} = 0$, $\overline{\beta}_{mn} = \delta_{m0}\delta_{n1}$ (δ is the Kronecker symbol). Then, because $a_0 = 1$ and $a_1 = a_2 = b_1 = b_2 = 0$, it follows from (22) that

$$kR \to \infty \Longrightarrow |D_1^a|, |D_1^b| = O[(1/(kR)^2] \tag{29}$$

We thus recover that ABC0 with $a_0 = 1$ is exact in normal incidence when Γ is planar.

3) Regarding ABC1 and ABC2, $a_0 = 1$ and $D_n^a = D_n^b = 0$ in (22) for $0 \le n \le n_M$ entail

$$\begin{aligned} &0 \le n \le n_M \\ \text{ABC1}:\ &xh_n(x) - i(1-\gamma_n a_2)\widetilde{h}_n(x) = 0 \\ &ixh_n(x)(1-\gamma_n a_1) + \widetilde{h}_n(x) = 0 \\ \text{ABC2}:\ &xh_n(x) - i(1-\gamma_n b_1)\widetilde{h}_n(x) = 0 \\ &ixh_n(x)(1-\gamma_n b_2) + \widetilde{h}_n(x) = 0 \end{aligned} \tag{30}$$

that implies $b_1 = a_2$, $b_2 = a_1$ and, consequently, $D_n^a(\text{ABC1}) = D_n^b(\text{ABC2})$, $D_n^a(\text{ABC2}) = D_n^b(\text{ABC1})$, which means, as for PA, that ABC1 and ABC2 have exactly the same efficiency. The least-squares solution of the ABC1 system in (30) gives the SA values of a_1 and a_2.

In this option, the curvature of Γ is implicitly taken into account by the ABC1 = ABC2 and ABC3 coefficients. It might be extended to more general surfaces with non-equal principal curvatures, such as the axisymmetric ellipsoid or spheroid, provided that the corresponding closed-form solution of Maxwell's equations, obtained via separation of variables, is prone to a simple enough numerical implementation.

2.3. Sufficient Uniqueness Conditions (SUCs) for Maxwell's Problem with HOABC on Γ

Sufficient uniqueness conditions for Maxwell's problem with HOABC (4) are easily obtained from those proposed in [22] with HOIBC (1):

$$\begin{aligned} &\text{SUC ABC0}:\ \text{Re}(a_0) > 0 \\ &\text{SUC ABC1}:\ \text{Re}(a_0) > 0;\ \text{Re}(a_1) \le 0;\ \text{Re}(a_2) \le 0 \\ &\text{SUC ABC2}:\ \text{Re}(a_0) > 0;\ \text{Re}(a_0^* b_1) \le 0;\ \text{Re}(a_0^* b_2) \le 0 \\ &\text{SUC ABC3}:\ z = 1 - a_2/a_1 - a_1/a_2 \\ &\text{Re}(a_1) \le 0;\ Re(a_2) \le 0;\ \text{Re}(a_1^* z) \le 0;\ \text{Re}(a_2^* z) \le 0 \\ &0 \le \text{Re}(a_1^* a_2) \le \frac{|a_1 a_2|^2}{|a_1|^2 + |a_2|^2} \end{aligned} \tag{31}$$

If $\mathbb{S}$ designates the subspace of $\mathbb{C}^5$, where χ satisfies the SUCs, then the coefficients are obtained from

$$\chi^{\text{PA}} = \arg\min_{\chi\in\mathbb{S}}\left\{\sum_{p=\text{TM,TE}}\sum_{i=1}^{N_{s_M}}|r^p(s_i,\chi)|\right\} \tag{32}$$

$$\chi^{\text{SA}} = \arg\min_{\chi\in\mathbb{S}}\left\{\sum_{n=1}^{n_M}(|D_n^a(\chi)| + |D_n^b(\chi)|)\right\} \tag{33}$$

We note that the ABCWK and ABC30 coefficients do not satisfy the ABC3 SUC. We emphasize that the SUCs in (31) are sufficient but not necessary: if they are satisfied, the solutions of Maxwell's problem with the HOABC are unique. However, they might be unique in the opposite case. Also, it is shown in Appendix C that $\mathrm{Re}(Z^p(s)) \geq 0$ for ABC1, ABC2, ABC3 if their coefficients satisfy the above SUCs, and (17) entails $s \leq 1 \Longrightarrow |r^p(s)| \leq 1$ for PA.

2.4. Numerical Evaluation of the ABCs' Performance

ABCs efficiencies are investigated first on an infinite plane and then on a sphere.

2.4.1. Γ is an Infinite Plane: ABCs Coefficients are Calculated with the Planar Approximation (PA)

The non-constrained coefficients a_1, a_2 are the least square solutions of systems (14) for ABC1 and (15) for ABC3, with $N_{s_M} = 100$. The constrained coefficients are computed via a computer program [26], based on a stochastic, gradient-free, cross-entropy method [25], in which constraints can be easily introduced and of which we recall the main lines. The cost function is $F(\chi) = |M\chi - b|$ where $\chi = (a_1, a_2)^t$, and M (respectively b) is the $(2N_{s_M} \times 2)$ matrix ($(2N_{s_M} \times 1)$ r.h.s., respectively) in (14) for ABC1 and in (15) for ABC3 (for the latter, $2N_{s_M}$ is replaced by N_{s_M}). Given initial mean value $\bar{\chi}_0$, set equal to the non-constrained value of χ and standard deviation σ_0, the iterative algorithm computes the minimum of $F(\chi)$: at iteration n, the mean value $\bar{\chi}_n$ and standard deviation σ_n corresponding to the minimum of $F(\chi)$ found at this iteration are calculated from N_r realizations verifying the SUCs in (31). The algorithm stops when σ_n is smaller than a given ε_σ. It is efficient when the size of χ is moderate. The result is stochastic, but the coefficient values converge when $\varepsilon_\sigma \to 0$ and $N_r \to \infty$. Finally, note that, as it happens for many minimization problems where $F(\chi)$ is not convex, this method does not necessarily find the absolute minimum. In what follows, the constrained coefficient values are obtained with $\sigma_0 = 0.5$, $N_r = 500$, and $\varepsilon_\sigma = 0.01$. The reflection coefficients are plotted for ABC0, ABC1, ABCWK, ABC3, and ABC30 in Fig. 1 for $s_M = 0.2$ and $s_M = 1.2$ (we recall that ABC2 has exactly the same effectiveness as ABC1) with the coefficients values reported in Table 1. A small value of s_M is advised if Γ is located far enough away from the object because the field impinging on Γ is then essentially propagative (very similar results are obtained for $s_M = 0.5$). We observe that as expected, ABC30 $=$ ABC3$(s_M = 0)$ and ABC3 w/o SUC display similar performances and are the most efficient.

– SUCs degrade ABCs' performance since χ spans a reduced parameter space (we recall that a well-posed problem is not guaranteed for ABCWK and ABC30).

– ABC3 w/SUC has the same effectiveness as ABC1 w/o SUC, and the latter has the same effectiveness as ABCWK $=$ ABC1$(s_M = 0)$.

– Bottom of Fig. 1 shows the reduced performances achieved by ABC3 with $s_M = 1.2$ to take into account evanescent waves on Γ.

TABLE 1. Values of a_1, a_2 obtained for $s_M = 0.2$ and 1.2. Non-constrained coefficients are the least-squares solutions of systems (14) for ABC1 and (15) for ABC3. Constrained coefficients are obtained via the cross-entropy technique.

s_M			w/o SUC	w/SUC
0.2	ABC1	a_1	0.503	$-0.0038 - i0.000173$
		a_2	-0.512	$-0.74 - i0.0036$
	ABC3	a_1	0.753	$-0.000643 + i0.0783$
		a_2	0.253	$-0.51 + i0.07235$
1.2	ABC1	a_1	$0.761 + 0.225i$	$-0.00174 + 0.218i$
		a_2	$-0.481 - 1.236i$	$-0.485 - 1.243i$
	ABC3	a_1	$0.935 + 0.128i$	$-0.0012 + 0.342i$
		a_2	$0.514 + 0.261i$	$-0.393 - 0.00131i$

2.4.2. The Object and Γ Are Concentric Spheres: ABCs Coefficients are Calculated with the Planar Approximation (PA) or the Spherical Approximation (SA)

We consider the scattering problem of a plane wave by a sphere of radius R_0, on which the impedance boundary condition

$$r = R_0 : \ \underline{E}_t = Z\underline{J} \tag{34}$$

is prescribed, coated with a material layer of thickness d_0, relative dielectric permittivity ε, and magnetic permeability μ. The radius of this coated sphere is $R_S = R_0 + d_0$, and impedance Z, normalized to free-space impedance, is known. Γ is a sphere of radius $R = R_0 + d_0 + d$. The solutions of this scattering problem with the exact and approximate (i.e., the ABC) radiation conditions are obtained in closed forms via the standard Mie series truncated at $n = N_{mie} = 8 + E(kR_S\sqrt{2})$ — as for the series in (20), (23) —, a large enough value to guarantee a very good numerical accuracy. Regarding SA, the non-constrained ABC1 and ABC3 coefficients are the solution of least-squares systems (30) and (28). The constrained coefficients are obtained via the cross-entropy technique as described in Section 2.4.1 with $F(\chi) = \sum_{n=1}^{n_M}(|D_n^a(\chi)| + |D_n^b(\chi)|)$ — see (33). Then, the ABCs' performances are numerically evaluated in terms of the far field $\underline{E}^0(\theta)$ by plotting the exact and ABCs bistatic Radar Cross Section in dBm^2

$$\mathrm{RCS}(\theta) = 10\log[4\pi|\underline{E}^0(\theta)|^2]; \ \underline{E}^0(\theta) = \lim_{r\to\infty} r\underline{E}^s(r,\theta)$$

(θ is the observation angle counted from the direction $\theta = 0$ of the incident plane wave) and computing the far-field error $errE^0(\theta)$ and its average $erravE^0$:

$$\begin{aligned} errE^0(\theta) &= \max_{p=\mathrm{TM,TE}} 10\log\left[4\pi\left|\underline{E}^{0,p}_{exact}(\theta) - \underline{E}^{0,p}_{\mathrm{ABC}}(\theta)\right|^2\right] \\ erravE^0 &= \frac{1}{\pi}\int_0^\pi errE^0(\theta)d\theta \end{aligned} \tag{35}$$

We consider successively the following lossy and lossless coatings: $\varepsilon = \mu = 1 - i$, $Z = 1$, $d = 5$ mm and $\varepsilon = 4$, $\mu = 2$, $Z = 0$, $d = 3$ mm. The PA ABCs' coefficients are those indicated in Table 1 for $s_M = 0.2$.

1) Lossy coating. Because $\varepsilon = \mu$ and $Z = 1$, Weston's theorem [28] implies that the exact radar cross-section (RCS)

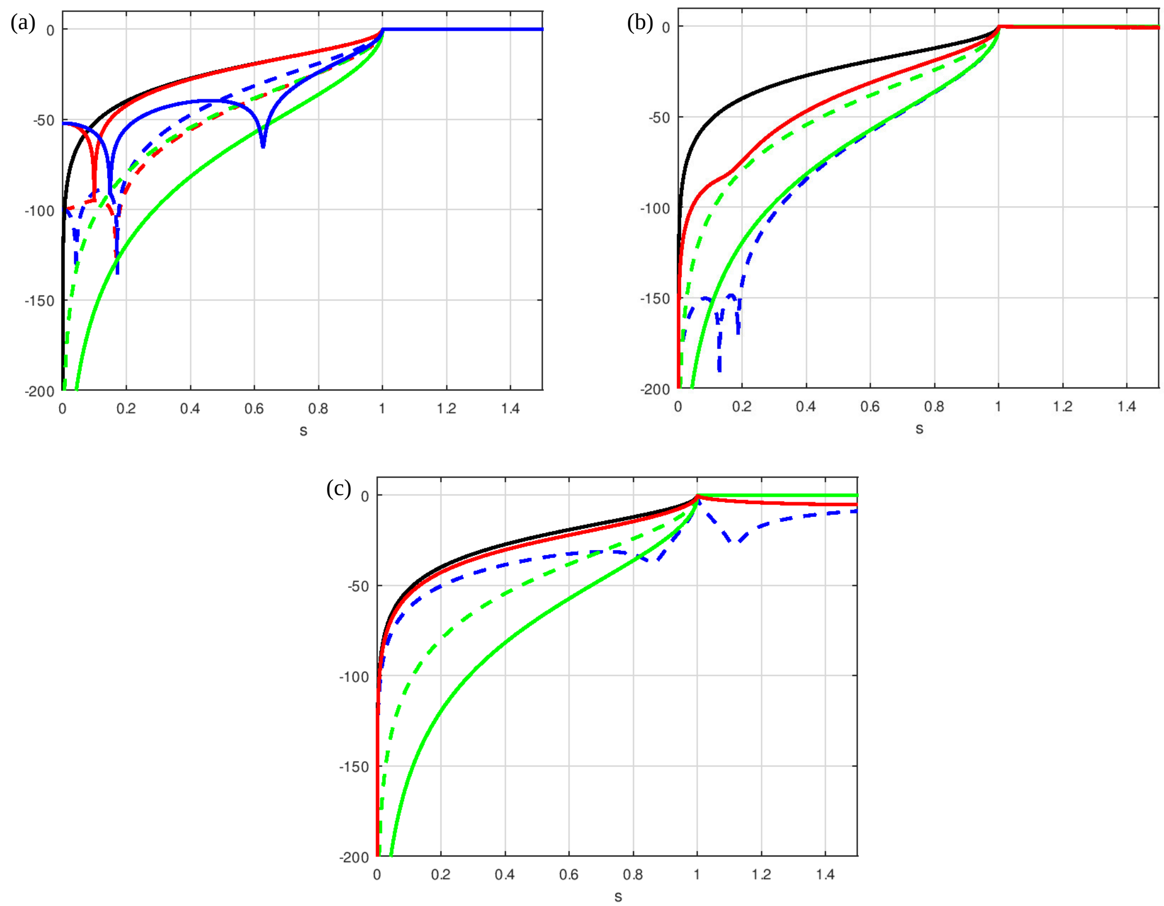

FIGURE 1. $20\log|r(s)|$. The plane Γ is illuminated by a plane wave with angle of incidence θ counted from the normal. Incident and reflected waves are propagative when $s = \sin\theta \leq 1$ and evanescent when $s > 1$. ABC0 (black, TM = TE), ABC30 (green solid line, TM=TE), ABCWK (green dashed line, TM=TE). (a) $s_M = 0.2$, ABC1 w/o SUC: dashed lines (TM: red, TE: blue); ABC1 w/SUC: solid lines (TM: red, TE: blue). (b) $s_M = 0.2$, ABC3 w/o SUC: blue dashed line; w/SUC: red solid line. (c) $s_M = 1.2$, ABC3 w/o SUC: blue dashed line; w/SUC: red solid line.

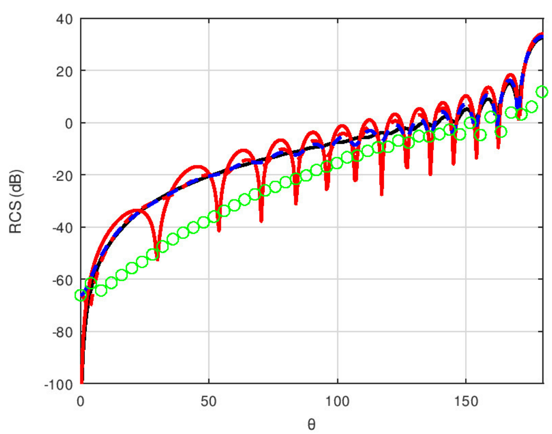

FIGURE 2. Sphere of radius $R_0 = 1$ m and IBC (34) with $Z = 1$, coated with the lossy material $\varepsilon = \mu = 1 - i$ of thickness $d_0 = 5$ mm. Γ is a concentric sphere of radius $R = R_0 + d_0 + d$ with $d = 1$ cm. The incident plane wave impinges on the sphere at $\theta = 0$ and $f = 1$ GHz. RCS(θ) for ABC0 (red), exact (black) and ABCWK (TM: dashed red line, TE: dashed blue line). $errE^0(\theta)$ (35) for ABCWK: green circles.

verifies $\mathrm{RCS}(0) = -\infty$ and is polarization independent. It is easily shown that these properties are also verified by the RCSs obtained with ABC0, ABC3, and ABC30. RCS and far-field error $errE^0$ achieved with the ABCs are plotted in Figs. 2–4. We have set $f = 1$ GHz, $R_0 = 1$ m, $d = 1$ cm, and the ABCs coefficients are those in Table 1, obtained via PA with $s_M = 0.2$ (lossy coating: propagative waves prevail on Γ). ABC30 is not shown because it has the same efficiency as ABC3 without SUC. As for PA (see comments in Section 2.4.1), we observe that ABC3 with SUC performs slightly better than ABC2 without SUC, which in turn performs as ABCWK. Very similar results are obtained for $s_M = 0.5$ (not shown). Finally, $erravE^0$ is plotted vs. f and d in Fig. 5, which displays the high accuracy achieved with ABC3 even when Γ is very close to the object. The errors obtained with ABC2 w/o SUC (not shown) and ABC3 w/SUC are similar.

ABC1 and ABC3 coefficients are now computed via SA to take the curvature into account. As above, $s_M = 0.2$, and for SA, (26) reads $n_M = E(0.2kR_S) + 1$. The far-field errors achieved with PA, SA, and ABCWK (whose coefficients are computed from (12) with $R = R_0 + d_0 + d$) are reported in Table 2 for $f = 1$ GHz, $d = 1$ cm, and three values of R_0. As expected, the accuracy achieved with PA and SA is very similar when $kR \gg 1$; otherwise, ABC3-SA is the most effective (see also Fig. 6). Also, ABC2-SA w/o SUC and ABCWK have a similar efficiency.

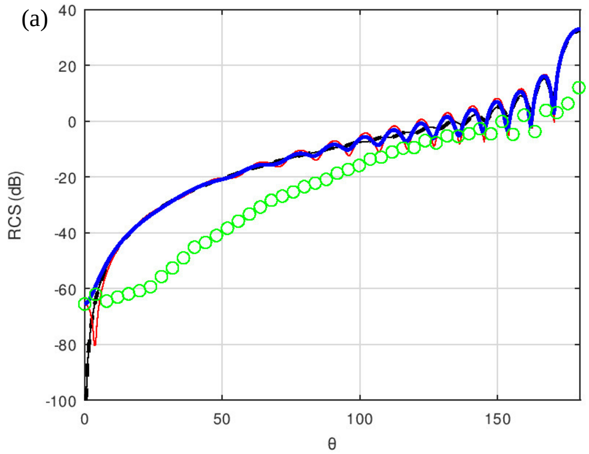

FIGURE 3. Same lossy sphere and spherical Γ as in Fig. 2 and $f = 1$ GHz. RCS(θ) and *errE*$^0(\theta)$ for ABC2-PA ($s_M = 0.2$) with $b_1 = a_2$, $b_2 = a_1$, as explained in Section 2.2, where a_1, a_2 are given in Table 1; red (blue): TM (TE respectively); exact: black; *errE*$^0(\theta)$: green circles. (a) w/o SUC and (b) w/SUC.

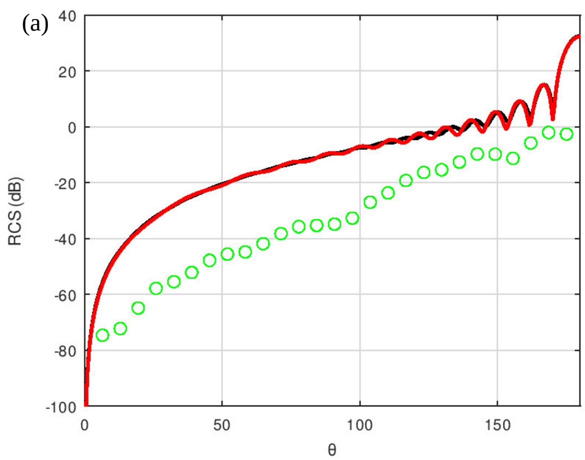

FIGURE 4. Same lossy sphere and spherical Γ as in Fig. 2 and $f = 1$ GHz. Performances of ABC3-PA with $s_M = 0.2$, (a) w/o SUC and (b) w/SUC. Exact RCS(θ): black; ABC3-PA RCS(θ): red. *errE*$^0(\theta)$: green circles.

2) Lossless coating. When this coating is planar, surface waves (SWs), also called guided waves [29], may exist, which propagate unattenuated along the plane and are evanescent in the normal direction z with amplitude proportional to $\exp\left(-kz\sqrt{s^2-1}\right)$ because of (6). In the $[1, 12]$ GHz frequency range, the simple technique proposed in [30] yields two SWs for $f = 2.2$ GHz ($f = 10.2$ GHz) with $s = 1.03$ in TM ($s = 1.01$ in TE, respectively).

When $kR \gg 1$, the SWs retain these characteristics in the spherical coating, but the SWs are attenuated when they circumscribe the sphere because of radiation losses. In particular, they are weakly evanescent in r, and the amplitude on Γ of the above-mentioned SWs is then proportional to $\exp\left(-kd\sqrt{s^2-1}\right)$, which explains why d must be larger when $f = 2.2$ GHz ($s = 1.03$, while $s = 1.01$ for $f = 10.2$ GHz), as observed on Fig. 7. In addition, since $s \simeq 1$, the SWs far-field contribution to the RCS is important [30], and these SWs cannot be accounted for by PA because of (18). When the ABC's coefficients are obtained via SA, the weight of evanescent waves in (25) must be increased accordingly:

$$\chi^{\mathrm{SA}} = \arg\min \left\{ \frac{\sum_{n=1}^{n_M} \left(|D_n^a(\chi)| + |D_n^b(\chi)|\right)}{n_M + 1} + \frac{\sum_{n=n_1}^{n_M} \left(|D_n^a(\chi)| + |D_n^b(\chi)|\right)}{n_M - n_1 + 1} \right\} \quad (36)$$

n_M is given by (26) with s_M equal to the values of s characterizing the SWs and $n_1 \le n_M$. Fig. 8 and Table 3 display the high accuracy achieved with SA for $d \ll 1$ at 2.2 GHz and 10.2 GHz when $n_1 = E(kR_S)$ and $n_M = E(1.03\, kR_S)+1$. This is made possible because $|D_n^a(\chi)| = |D_n^b(\chi|)$ — see (27) — can be much smaller than 1 when $n_1 \le n \le n_M$ as observed on Fig. 9,

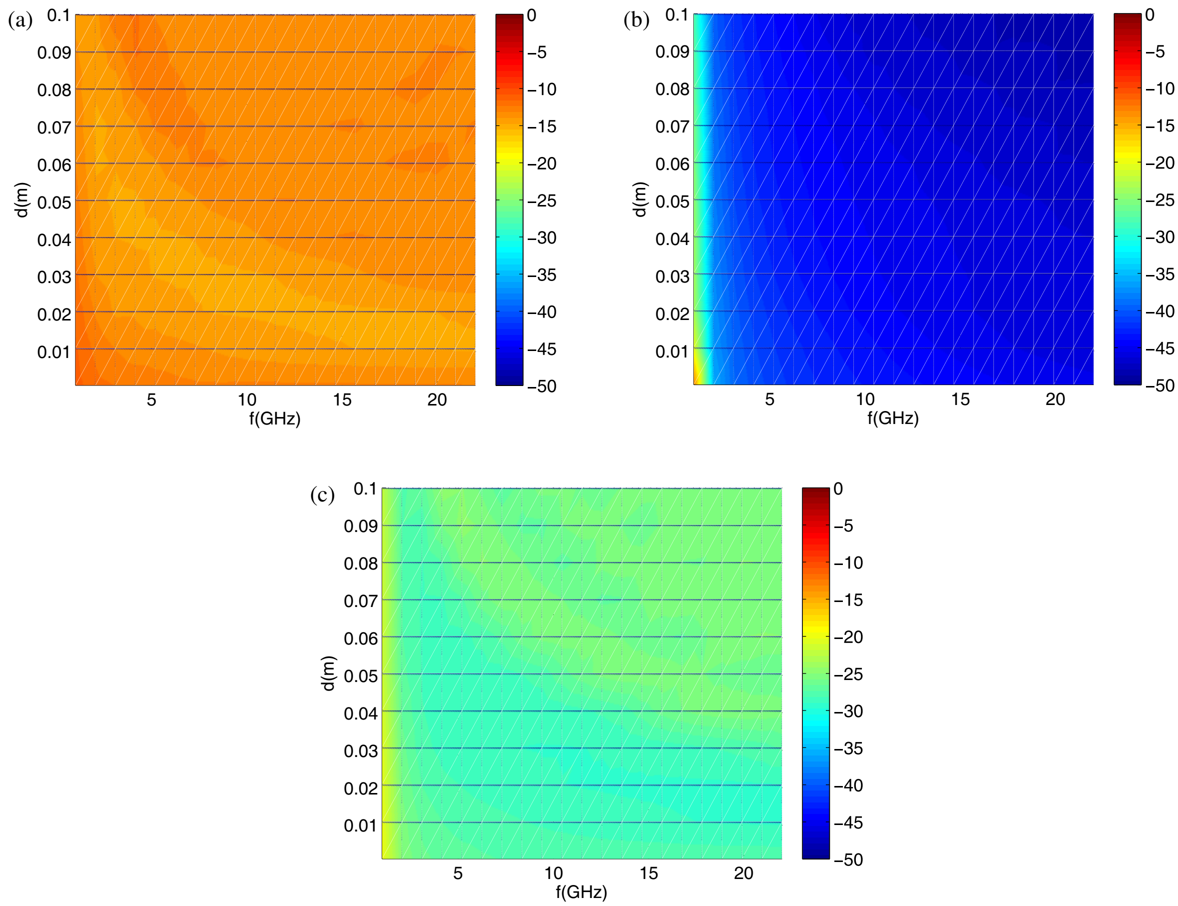

FIGURE 5. Same lossy sphere and spherical Γ as in Fig. 2. Far field average error *erravE*^{0} vs. f and d: (a) ABC0, (b) ABC3-PA ($s_M = 0.2$) w/o SUC, and (c) ABC3-PA ($s_M = 0.2$) w/SUC.

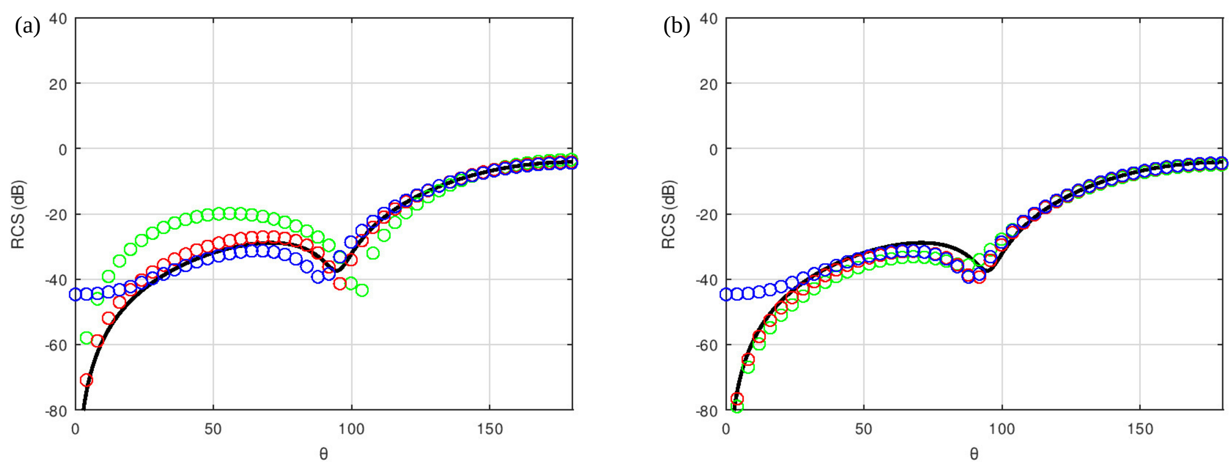

FIGURE 6. RCS(θ). Lossy coating, $R_0 = 0.1$ m, $d = 1$ cm, $f = 1$ GHz. Exact: black solid line; ABCWK with $R = R_0 + d_0 + d$ in (12): blue circles. ABC3-PA ($s_M = 0.2$): green circles. ABC3-SA ($n_M = 1$): red circles. (a) w/o SUC, (25) yields for SA: $a_1 = 0.6513 + 0.377$i, $a_2 = 0.2454 + 0.2523$i and (b) w/SUC, (33) yields for SA: $a_1 = -0.0616 + 0.31$i, $a_2 = -0.581 + 0.114$i.

contrary to PA when Γ is a plane: because of (18) the reflection coefficient is very close to unity when $s \simeq 1$. We recall, as observed in Table 2, that (i) ABC30, ABC3-PA, and ABC3-SA with $s_M = 0.2$ have the same effectiveness when $kR \gg 1$ and (ii) ABC3-PA w/SUC and ABCWK perform similarly while ABC3-PA w/o SUC is much more effective than ABCWK. Finally, the strong RCS oscillations observed in Fig. 8 in the forward scattering region in TM result from interferences between reflected rays and evanescent SW rays launched tangentially to Γ, as illustrated in [30]. Actually, an estimation of the SWs resonance frequencies and of the corresponding value of s_M is obviously not easily available for an arbitrary object. However,

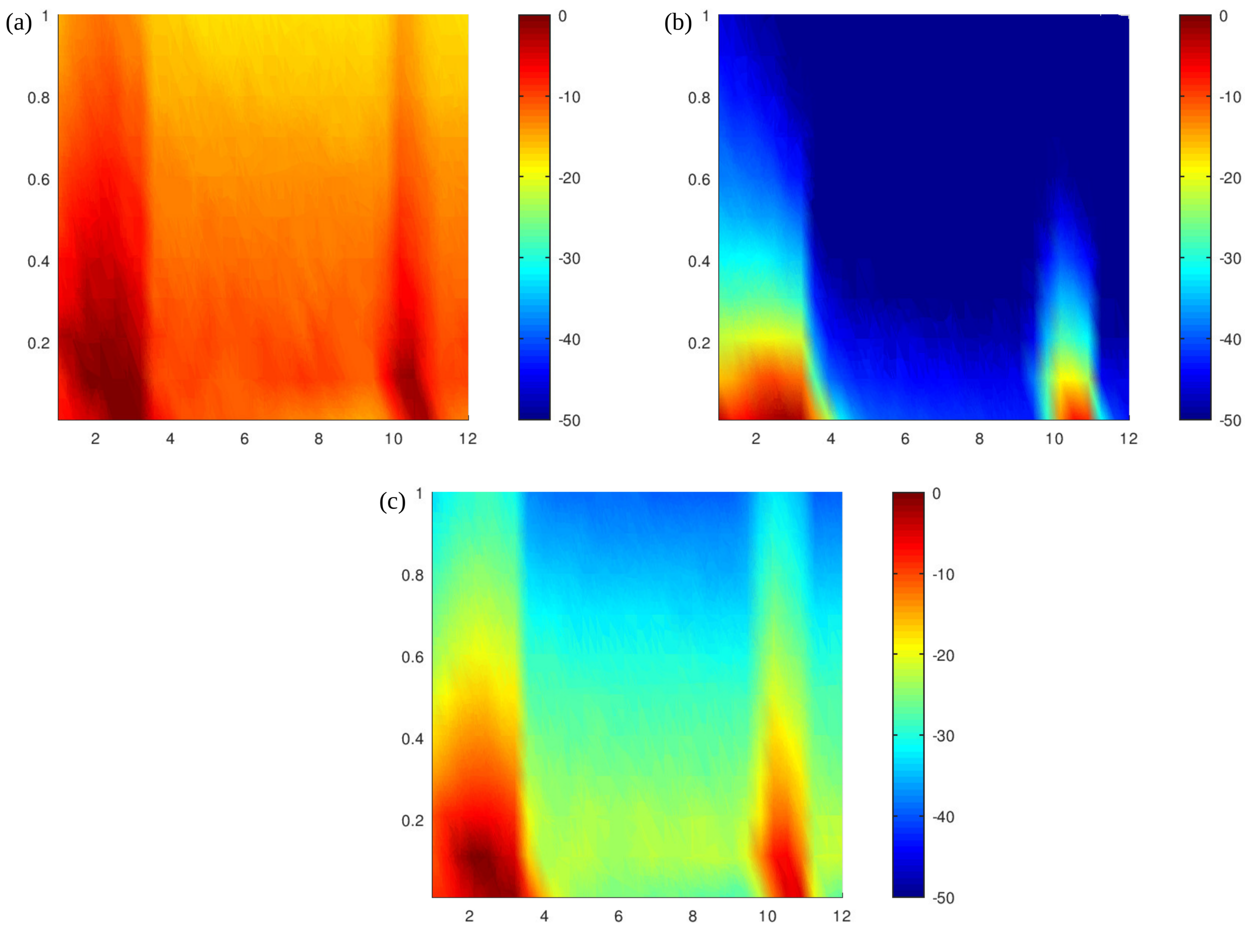

FIGURE 7. Lossless coating ($\varepsilon = 4$, $\mu = 2$, $Z = 0$, $R_0 = 1\,\mathrm{m}$, $d_0 = 3\,\mathrm{mm}$). Far field global error $erravE^0(f, d)$ with $f \in [1\,\mathrm{GHz}, 12\,\mathrm{GHz}]$ and $d \in [0.01\,\mathrm{m}, 1\,\mathrm{m}]$. SWs exist in the coating, which strongly radiate at 2.2 GHz (in TM, $s = 1.03$) and 10.2 GHz (in TE: $s = 1.01$). (a) ABC0, (b) ABC3-PA ($s_M = 0.2$) w/o SUC, and (c) ABC3-PA ($s_M = 0.2$) w/SUC.

TABLE 2. Same lossy sphere and spherical Γ as in Fig. 2, $f = 1\,\mathrm{GHz}$, average far-field error for ABC0, ABCWK, ABC2 and ABC3. PA: $s_M = 0.2$; SA: $n_M = E(0.2kR_S) + 1$. As explained in Section 2.2, for ABC0 $a_0 = 1$ yields the best results on a spherical Γ.

R_0 (m)	ABCno	SUC	$erravE^0$ PA	$erravE^0$ SA	$erravE^0$ ABCWK
2	0	-	-8.15	-	-18.6
	2	w/o	-19.7	-19.1	
		w/	-6.5	-6.4	
	3	w/o	-32.1	-42.7	
		w/	-21.2	-20.3	
1	0	-	-14.6	-	-23.5
	2	w/o	-24.7	-24.1	
		w/	-12.4	-12.2	
	3	w/o	-34.2	-43.9	
		w/	-26.5	-25.7	
0.1	0	-	-35	-	-38
	2	w/o	-32.8	-38.8	
		w/	-31.5	-33.2	
	3	w/o	-29.5	-46	
		w/	-39.7	-43	

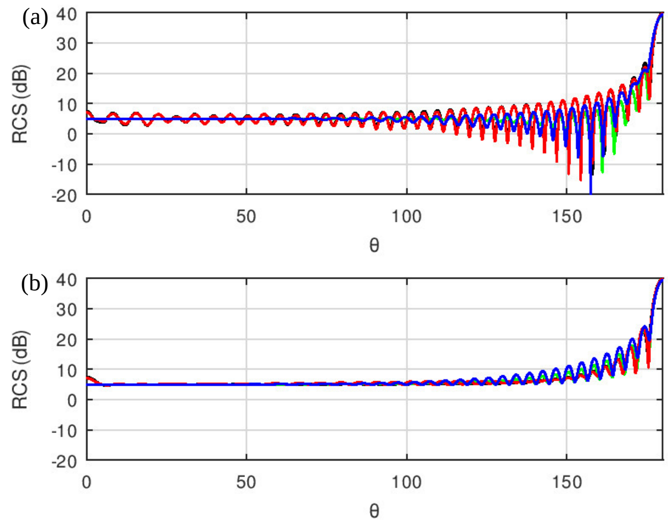

FIGURE 8. Lossless coating, $d = 1$ cm, $f = 2.2$ GHz, $kR = 46.7$, RCS(θ). ABC3 w/o SUC and ABCWK. **TOP** (**BOTTOM**): TM (TE). Exact: black; PA ($s_M = 0.2$): green; ABCWK: blue; SA with $n_1 = E(kR_0) = 47$ and $n_M = E(1.03kR_S) + 1 = 49 \Longrightarrow a_1 = 0.926 + 0.11\text{i}$, $a_2 = 0.529 + 0.245\text{i}$: red (superimposed on the exact RCS).

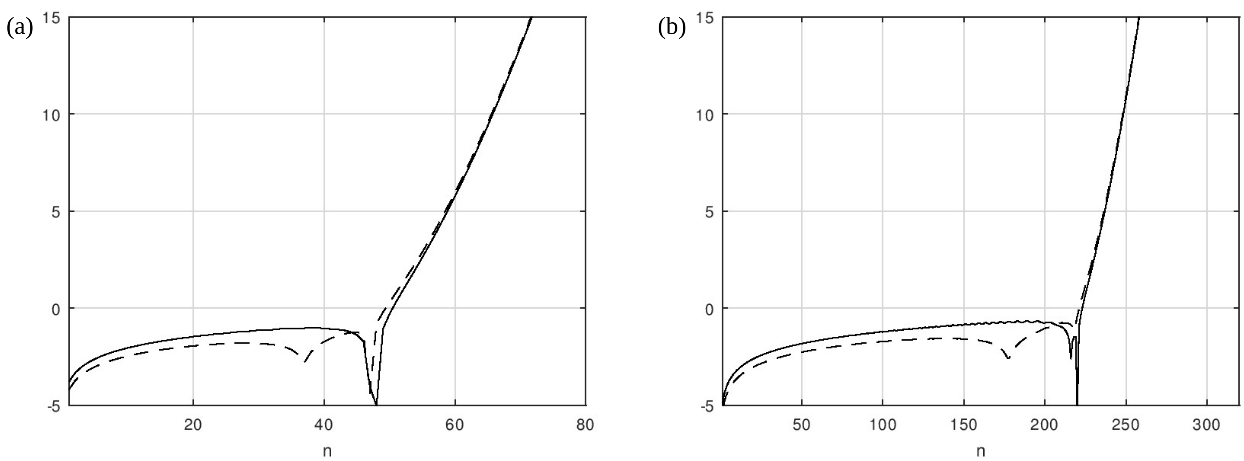

FIGURE 9. Lossless coating, $d = 1$ cm, $\log |D_a(n)|$, ABC3 w/o SUC, SA. Solid line: (36) with $n_1 = E(kR_S)$ and $n_M = E(1.03kR_S) + 1$; dahed line: (25) with $n_M = E(1.03kR_S) + 1$. (a) $f = 2.2$ GHz. (36) with $n_1 = 47$, $n_M = 49 \Longrightarrow$ same values of a_1, a_2 as in Fig. 8. (25) with $n_M = 49 \Longrightarrow a_1 = 0.896 + 0.102i$, $a_2 = 0.451 + 0.137\text{i}$. (b) $f = 10.2$ GHz. (36) with $n_1 = 217$, $n_M = 223 \Longrightarrow a_1 = 0.975 + 0.04634\text{i}$, $a_2 = 0.708 + 0.184\text{i}$. (25) with $n_M = 223 \Longrightarrow a_1 = 0.948 + 0.0553\text{i}$, $a_2 = 0.544 + 0.0911\text{i}$.

TABLE 3. Lossless coating: *erravRCS*(d) for the ABCs. For both frequencies $s_M = 0.2$ for ABC3-PA and $s_M = 1.03$ for ABC3-SA (the corresponding values w/o SUC of a_1, a_2 for $d = 0.01$ m are indicated in Fig. 9 captions).

f (GHz)	d (m)	ABC0	ABCWK	ABC3-PA w/o SUC	ABC3-PA w/SUC	ABC3-SA w/o SUC	ABC3-SA w/SUC
2.2	0.001	−1.1	−3.1	−3.7	−3	−19	−2.2
	0.01	−1.5	−3.1	−3.8	−3	−18.7	−2.5
	0.1	5.5	0.7	−9.5	0.6	−33.2	−7.3
	0.5	−5.6	−16.1	−35.2	−16.2	−62.3	−25.2
	1	−11.4	−27.9	−48.1	−28	−81.2	−35.4
10.2	0.001	−5.6	−10.2	−12.3	−9.9	−16.6	−5.7
	0.01	−6.5	−11	−12.4	−10.3	−18.8	−7.6
	0.1	0.34	−8.4	−17.2	−5.1	−39.8	−12.5
	0.5	−8	−23.2	−43.9	−19.6	−66.8	−27.7
	1	−13	−33.7	−60.8	−31	−84.5	−37.3

when lossless materials are present all along the object surface, resonant circumferential waves might be expected, and a planar analysis of the coating, such as the one presented here, can be useful. Finally, let us mention that the choice of a large enough value of $s_M > 1$ to account for possible evanescent waves on Γ in the whole frequency range is not acceptable because, for the coated sphere considered here and $s_M = 1.2$, ABC3-SA yields large errors: *erravE*$^0 = 0.6$ w/o SUC and *erravE*$^0 = 3.7$ w/SUC.

3. CONCLUSIONS

As far as we know, contrary to the HOABCs published in the past, ABC3 and, to a lesser extent, ABC1 that we have shown to be strictly equivalent to ABC2 in terms of effectiveness, yield a high numerical accuracy even when Γ is very close to a coated sphere, and SUCs have been proposed that guarantee a well-posed problem at the cost of reduced ABC1 and ABC3 performances; it is however important to note that ABC3 w/SUC is still more effective than ABC1 w/o SUC.

When mostly propagating waves are present on Γ, the planar approximation (PA) with $s_M = 0.2$ is sufficient: PA can be used on an arbitrary boundary provided that the local tangent plane approximation is justified; otherwise Γ is a sphere whose radius is taken into account by the ABC3 coefficients via the spherical approximation (SA), much more effectively than with the ABCWK in [17]. When strong evanescent waves are present on Γ, as is the case for the lossless coating at a resonance frequency of a surface wave, a good accuracy is achieved with SA on a spherical Γ only.

Also, we have shown that ABC3 with $s_M = 0$ yields ABC30 that has been independently derived from the exact ABC obtained on a planar Γ in Appendix B: ABC30 can be considered as the 3D vector equivalent of the third approximation of the exact 2D scalar ABC proposed in [13]. The numerical implementation of ABC1 and ABC3 in the FE domain decomposition method presented in [6, 7] and its performance evaluation on real-life objects are currently underway. The numerical complexity of the corresponding FE formulation is expected to be low while avoiding the introduction of additional unknowns, similar to that of the HOIBC presented in [22].

ACKNOWLEDGEMENT

We thank O. Cessenat for having fixed computer science issues, M. Lecouvez for carefully proofreading this manuscript and P. Minvielle for his cross-entropy minimization computer program.

APPENDIX A. $Z^{\mathrm{TM}} = 1/Z^{\mathrm{TE}}$ MINIMIZES $\sum_{P=\mathrm{TM,TE}} |R^P(S,\chi)|$

For a given ξ, let $Z_1 = Z^{\mathrm{TM}}$, $Z_2 = Z^{\mathrm{TE}}$ and

$$f(Z_1, Z_2) = \sum_{p=\mathrm{TM,TE}} |r^p| = \left|\frac{Z_1-\xi}{Z_1+\xi}\right| + \left|\frac{\xi Z_2 - 1}{\xi Z_2 + 1}\right| \quad \text{(A1)}$$

We have

$$f(Z_1, Z_2) = f(1/Z_2, 1/Z_1) \quad \text{(A2)}$$

Taking a cue from the approach presented in [31] for the isotropic case ($Z_1 = Z_2$), let $x_1(Z_1, Z_2) = Z_1 + 1/Z_2$, $x_2(Z_1, Z_2) = Z_2 + 1/Z_1$ and $g(x_1(Z_1, Z_2), x_2(Z_1, Z_2)) = f(Z_1, Z_2)$. g verifies (38): $g(x_1(Z_1, Z_2), x_2(Z_1, Z_2)) = g(x_1(1/Z_2, 1/Z_1), x_2(1/Z_2, 1/Z_1))$. Then, an extremum of f is obtained for

$$\partial_{Z_1} g = \partial_{x_1} g - Z_1^{-2}\partial_{x_2} g = 0;\ \partial_{Z_2} g = -Z_2^{-2}\partial_{x_1} g + \partial_{x_2} g = 0$$

that yields $(1 - Z_1^2 Z_2^2)\partial_{x_1} g = (1 - Z_1^2 Z_2^2)\partial_{x_2} g = 0$ which is satisfied if $Z_1 Z_2 = \pm 1$. $Z_1 Z_2 = -1$ is discarded since it implies $\mathrm{Re}(Z_1)\mathrm{Re}(Z_2) \le 0$, and it is well known that the solutions of Maxwell's problem are unique if $\mathrm{Re}(Z_1), \mathrm{Re}(Z_2) \ge 0$.

APPENDIX B. EXACT ABC OPERATOR ON A PLANAR Γ AND ABC30

The exact ABC operator is obtained as follows from the exact IBC derived in [23] on the surface Γ of a (ε, μ) layer with thickness d backed by a perfect electric conductor (PEC). Γ is the (xOy) plane, and the PEC plane is at $z = -d$. Equation (6) in [23] reads with $\underline{n} = \underline{z}$

$$\begin{aligned} &\Lambda(\underline{n} \times \underline{E}) = -i\eta \tan(k_m d\Lambda)(1 - L_R/k_m^2)H_t \text{ on } \Gamma \\ &\Lambda = \sqrt{1+t_1};\ t_1 = (L_D - L_R)/k_m^2;\ k_m = k\sqrt{\varepsilon\mu}; \\ &\eta = \sqrt{\mu/\varepsilon} \end{aligned} \quad \text{(B1)}$$

To derive the ABC from (B1), we consider a weakly lossy free-space material: $\varepsilon = \mu = 1 - i\varepsilon''$ with $0 < \varepsilon'' \ll 1$, and we let $d \to \infty$. Because $k_m^2 = k_{mx}^2 + k_{mz}^2$ with $k_{mx} = sk_m$, we have $k_{mz} = k_m\sqrt{1-s^2}$ and the field reflected by Γ — which propagates towards negative z for $s \le 1$ and behaves (in the conventions of [23]) as $e^{izk_{mz}}$ — must be bounded when $z \to -\infty$. We have $k_m = k_m' + ik_m''$ with $k_m' > 0$ and $k_m'' < 0$. Then, because $t_1 = -s^2 \in \mathbb{R}$, $\lim_{d\to\infty} \tan(k_m d\Lambda) = -i$ and (B1) yields, when $\varepsilon'' = 0$, the following exact ABC

$$\Lambda\underline{n} \times \underline{E} = -(1 - L_R/k^2)\underline{H}_t \quad \text{(B2)}$$

For convenience sake, we perform $\underline{n}\times$ (B2). We note that (i) $\underline{H}_t = -\underline{n} \times \underline{J}$, (ii) $\underline{n} \times (\Lambda\underline{n} \times \underline{E}) = \Lambda(\underline{n} \times \underline{n} \times \underline{E}) = -\Lambda\underline{E}_t$ since Λ can be replaced by its formal Taylor series expansion in terms of $(L_D - L_R)/k^2$, (iii) $\underline{n} \times L_R(\underline{n} \times \underline{J}) = L_D\underline{J}$, so that the exact ABC (B2) also reads

$$\Lambda\underline{E}_t = (1 + L_D/k^2)\underline{J} \quad \text{(B3)}$$

To obtain the exact Z^{TE}, we note that in TE polarization, $L_D J = 0$, $L_D E_t = 0$, $L_R E_t = k^2 s^2 E_t$, so that (B3) yields $\sqrt{1-s^2}E_t = J$ and $Z^{\mathrm{TE}} = (1-s^2)^{-1/2}$. Then, $Z^{\mathrm{TM}} = 1/Z^{\mathrm{TE}} = \sqrt{1-s^2}$, of which the Padé (2,2) approximant centered at $s = 0$ is $\dfrac{1 - 3s^2/4}{1 - s^2/4}$, which yields the ABC30 coefficients in (12).

APPENDIX C. FOR ABC1, ABC2 AND ABC3 THE SUC IMPLY $\mathrm{RE}(Z^P(S)) \geq 0$ FOR $P = \mathrm{TM}, \mathrm{TE}$

For $z \in \mathbb{C}$, we note here $z' = \mathrm{Re}(z)$ and $z'' = \mathrm{Im}(z)$. We consider TM polarization (TE follows along the same lines).

— ABC1: (31) implies $a_1' \leq a_0'/s^2$ that in turn entails $Z' \geq 0$.

— ABC2: $Z' = \dfrac{a_0' - (a_0 b_1^*)' s^2}{|1 - b_1 s^2|^2}$ and (31) implies $a_0' - (a_0 b_1^*)' s^2 \geq 0$.

— ABC3: $Z' = \dfrac{1 - (a_1' + a_2')s^2 + (a_1 a_2^*)' s^4}{|1 - a_2 s^2|^2}$ and (31) implies $1 - (a_1' + a_2')s^2 + (a_1 a_2^*)' s^4 \geq 0$.

REFERENCES

[1] Nedelec, J. C., "Mixed finite elements in $\mathbb{R}^3$," *Numerische Mathematik*, Vol. 35, No. 3, 315–341, 1980.

[2] Jin, J.-M., *The Finite Element Method in Electromagnetics*, John Wiley & Sons, 2015.

[3] Monk, P., *Finite Element Methods for Maxwell's Equations*, Oxford University Press, NY, USA, 2003.

[4] Yuan, X., "Three-dimensional electromagnetic scattering from inhomogeneous objects by the hybrid moment and finite element method," *IEEE Transactions on Microwave Theory and Techniques*, Vol. 38, No. 8, 1053–1058, 1990.

[5] Guan, J., S. Yan, and J.-M. Jin, "An accurate and efficient finite element-boundary integral method with GPU acceleration for 3-D electromagnetic analysis," *IEEE Transactions on Antennas and Propagation*, Vol. 62, No. 12, 6325–6336, 2014.

[6] Stupfel, B. and M. Lecouvez, "One-way domain decomposition method with exact radiation condition and fast GMRES solver for the solution of Maxwell's equations," *Journal of Computational Physics*, Vol. 322, 882–904, 2016.

[7] Stupfel, B. and M. Chanaud, "High-order transmission conditions in a domain decomposition method for the time-harmonic Maxwell's equations in inhomogeneous media," *Journal of Computational Physics*, Vol. 372, 385–405, 2018.

[8] Berenger, J.-P., "A perfectly matched layer for the absorption of electromagnetic waves," *Journal of Computational Physics*, Vol. 114, No. 2, 185–200, 1994.

[9] Sacks, Z. S., D. M. Kingsland, R. Lee, and J.-F. Lee, "A perfectly matched anisotropic absorber for use as an absorbing boundary condition," *IEEE Transactions on Antennas and Propagation*, Vol. 43, No. 12, 1460–1463, 1995.

[10] Chew, W. C. and W. H. Weedon, "A 3D perfectly matched medium from modified Maxwell's equations with stretched coordinates," *Microwave and Optical Technology Letters*, Vol. 7, No. 13, 599–604, 1994.

[11] Mittra, R. and U. Pekel, "A new look at the perfectly matched layer (PML) concept for the reflectionless absorption of electromagnetic waves," *IEEE Microwave and Guided Wave Letters*, Vol. 5, No. 3, 84–86, 1995.

[12] Wilcox, C. H., "An expansion theorem for electromagnetic fields," *Communications on Pure and Applied Mathematics*, Vol. 9, No. 2, 115–134, 1956.

[13] Engquist, B. and A. Majda, "Absorbing boundary conditions for the numerical simulation of waves," *Mathematics of Computation*, Vol. 31, No. 139, 629–651, 1977.

[14] Higdon, R. L., "Absorbing boundary conditions for difference approximations to the multidimensional wave equation," *Mathematics of Computation*, Vol. 47, No. 176, 437–459, 1986.

[15] Bayliss, A. and E. Turkel, "Radiation boundary conditions for wave-like equations," *Communications on Pure and Applied Mathematics*, Vol. 33, No. 6, 707–725, 1980.

[16] Peterson, A. F., "Absorbing boundary conditions for the vector wave equation," *Microwave and Optical Technology Letters*, Vol. 1, No. 2, 62–64, 1988.

[17] Webb, J. P. and V. N. Kanellopoulos, "Absorbing boundary conditions for the finite element solution of the vector wave equation," *Microwave and Optical Technology Letters*, Vol. 2, No. 10, 370–372, 1989.

[18] Stupfel, B., "Absorbing boundary conditions on arbitrary boundaries for the scalar and vector wave equations," *IEEE Transactions on Antennas and Propagation*, Vol. 42, No. 6, 773–780, 1994.

[19] Wu, J.-Y., D. M. Kingsland, J.-F. Lee, and R. Lee, "A comparison of anisotropic PML to Berenger's PML and its application to the finite-element method for EM scattering," *IEEE Transactions on Antennas and Propagation*, Vol. 45, No. 1, 40–50, 1997.

[20] Stupfel, B., "A study of the condition number of various finite element matrices involved in the numerical solution of Maxwell's equations," *IEEE Transactions on Antennas and Propagation*, Vol. 52, No. 11, 3048–3059, 2004.

[21] Shin, W. and S. Fan, "Choice of the perfectly matched layer boundary condition for frequency-domain Maxwell's equations solvers," *Journal of Computational Physics*, Vol. 231, No. 8, 3406–3431, 2012.

[22] Stupfel, B., P. Payen, and O. Lafitte, "A well-posed and effective high-order impedance boundary condition for the time-harmonic scattering problem from a multilayer coated 3-D object," *Progress In Electromagnetics Research B*, Vol. 94, 127–144, 2021.

[23] Marceaux, O. and B. Stupfel, "High-order impedance boundary conditions for multilayer coated 3-D objects," *IEEE Transactions on Antennas and Propagation*, Vol. 48, No. 3, 429–436, 2000.

[24] Jones, D. S., *Acoustic and Electromagnetic Waves*, Clarendon Press, Oxford/New York, 1986.

[25] Kroese, D. P., S. Porotsky, and R. Y. Rubinstein, "The cross-entropy method for continuous multi-extremal optimization," *Methodology and Computing in Applied Probability*, Vol. 8, No. 3, 383–407, 2006.

[26] Minvielle, P., E. Tantar, A.-A. Tantar, and P. Berisset, "Sparse antenna array optimization with the cross-entropy method," *IEEE Transactions on Antennas and Propagation*, Vol. 59, No. 8, 2862–2871, 2011.

[27] Harrington, R. F., *Time-Harmonic Electromagnetic Fields*, Wiley-IEEE Press, 2001.

[28] Weston, V., "Theory of absorbers in scattering," *IEEE Transactions on Antennas and Propagation*, Vol. 11, No. 5, 578–584, 1963.

[29] Kong, J. A., *Electromagnetic Wave Theory*, John Wiley & Sons, New York, 1986.

[30] Stupfel, B., "Characterization of surface waves in a multilayer coating — Application to far-field control," *IEEE Transactions on Antennas and Propagation*, Vol. 69, No. 6, 3623–3627, 2021.

[31] Osipov, A. V., "Electromagnetic scattering from impedance-matched bodies," in *2015 9th European Conference on Antennas and Propagation (EuCAP)*, 1–3, Lisbon, Portugal, Apr. 2015.